

On the Joint Impact of Beamwidth and Orientation Error on Throughput in Directional Wireless Poisson Networks

Jeffrey Wildman, *Member, IEEE*, Pedro H. J. Nardelli, *Member, IEEE*,
Matti Latva-aho, *Senior Member, IEEE*, Steven Weber, *Senior Member, IEEE*

Abstract—We introduce a model for capturing the effects of beam misdirection on coverage and throughput in a directional wireless network using stochastic geometry. In networks employing ideal sector antennas without sidelobes, we find that concavity of the orientation error distribution is sufficient to prove monotonicity and quasi-concavity (both with respect to antenna beamwidth) of spatial throughput and transmission capacity, respectively. Additionally, we identify network conditions that produce opposite extremal choices in beamwidth (absolutely directed versus omni-directional) that maximize the two related throughput metrics. We conclude our paper with a numerical exploration of the relationship between mean orientation error, throughput-maximizing beamwidths, and maximum throughput, across radiation patterns of varied complexity.

Index Terms—wireless; directional antennas; beamforming; orientation error; stochastic geometry; transmission capacity; spatial throughput.

I. INTRODUCTION

IN a wireless communications network, directional antennas can help increase received signal power while simultaneously reducing interference. Antenna arrays that are steerable mechanically, electrically, or via switched-beams, can further improve networks performance by dynamically redirecting transmitted energy based on the network state. The performance analysis of directional antennas in large scale wireless communications systems over the last few decades has made use of a variety of models, assumptions, and analytical tools. However, much of the previous work assumes either perfect sector selection or beamsteering.

We anticipate the presence of several tradeoffs affecting network throughput and transmission capacity as antenna beamwidth decreases, stemming from sources of imperfect antenna configuration, beamforming, and selection [1]–[5]. Assuming constant transmitted power, decreasing beamwidth will result in a higher gain within the antenna’s main beam. As the beamwidth decreases, fewer interferers significantly affect the typical receiver, but their individual effects are stronger.

This work has been funded by the National Science Foundation (CNS-1147838) and the Academy of Finland.

J. Wildman and S. Weber are with the Department of Electrical and Computer Engineering, Drexel University, Philadelphia, PA USA (email: wildman@drexel.edu and sweber@ece.drexel.edu).

P. Nardelli and M. Latva-aho are with the Center for Wireless Communications (CWC), University of Oulu, Finland (email: nardelli@ee.oulu.fi and matti.latva-aho@ee.oulu.fi).

S. Weber is the corresponding author.

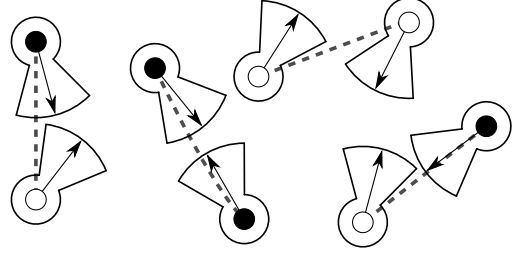


Fig. 1: A wireless network with directional antennas employed on transmitter and receiver pairs (dotted lines). When subjected to orientation error, transmitters and receivers may correctly direct their beam (black nodes), or they may miss their intended counterpart (white nodes).

Additionally, as the beamwidth decreases, properly aligning the transmitter and receiver becomes more difficult, but when both are aligned, the desired signal strength increases.

In this work, we study these tradeoffs in an ad hoc wireless network setting, modeled by a bipolar Poisson Point Process (PPP). We employ stochastic geometry to investigate optimal beamwidths that maximize throughput-based metrics in the presence of an assumed orientation error distribution. We now categorize and review related work in this area.

A. Related Work

Early works [6], [7] have studied the maximum throughput and expected forward progress of ALOHA and Carrier Sense Multiple Access (CSMA) systems using the protocol model with appropriately chosen interference zones. In particular, under Poisson ALOHA networks with antenna beamwidth β , C.-J. Chang and J.-F. Chang [6] found that certain routing schemes achieve a maximum throughput gain on the order of $\frac{1}{\beta}$. A second set of works [8]–[12] focused on throughput capacity of directional wireless networks, extending the seminal work of Gupta and Kumar [13]. Specifically, Yi *et al.* [9] found throughput gains of $O\left(\frac{1}{\alpha\beta}\right)$ in random networks employing the protocol interference model with transmitter and receiver beamwidths of α and β , respectively.

More recently, several works [14]–[17] have analyzed directional wireless networks with stochastic geometry, which offers a rich framework [18] for modeling effects such as physical interference (SINR) and fading. Hunter *et al.* [14]

studied spatial diversity schemes in ad hoc networks and found that static transmit and receive beamforming with M ideal sector antennas without sidelobes yields transmission capacity gains of $\Theta(M^2)$ over omni-directional antennas. Singh *et al.* [15] developed insights into medium access control design for highly directional networks by examining outage using protocol and physical interference models. Wang and Reed [16] incorporated directional antennas into the analysis of coverage in multi-tier heterogeneous cellular networks. Akoum *et al.* [17] were motivated by the rise of millimeter wave (mmWave) technology and studied achievable coverage and rates of mmWave beamsteering.

All of the works reviewed thus far assumed either perfect sector selection or perfect beamsteering. Even the *point-to-destination* scheme of C.-J. Chang and J.-F. Chang [6] modeled perfect orientation towards the destination, despite leading to outages when no feasible next hop falls within the transmitter's sector. We note that antenna orientation error can affect the distribution of gains between interferers and the typical receiver. While gain distributions have been used to study the interaction between arbitrary interferers and the typical receiver [16], [17], we are aware of no work that incorporates orientation error into a stochastic geometry based analysis.

However, we note several works that do explicitly account for error in directional wireless networks [3], [19]–[21]. Specifically, the effect of beam-pointing error can be associated with an averaged, normalized radiation pattern with a wider main lobe and higher sidelobes than the original normalized pattern without error [19], [20]. Shen and Pearson [19] investigated coupled oscillator beam-steering arrays and the effects of per-array-element phase error on beam-pointing error. Li *et al.* [20] discussed uniform linear array (ULA) beamforming error stemming from direction of arrival (DOA) estimation, spatial (or angular) spread of the transmitted signal, antenna array element perturbation, and mutual coupling of array elements. They analyzed outage and noted a degradation in performance due to error sources of increasing magnitude. Vakilian *et al.* [21] studied the impact of DOA estimation error, angular spread, and beamwidth on bit error rate. They noted that narrow beamwidths can exhibit higher bit error rates than wider beamwidths when subjected to a large enough DOA error.

B. Contributions

The rest of this paper is summarized as follows. §II introduces our wireless network model. §III explores the success probability of a typical transmitter under arbitrary radiation patterns (Prop. 1) and sectorized patterns (Cor. 2 and Cor. 3). §IV and §V study network metrics spatial throughput and transmission capacity, respectively. We derive closed form expressions for spatial throughput (Prop. 2) and transmission capacity (Prop. 4) under ideal sector antennas without sidelobes and arbitrary orientation error distributions. We find that concavity of the cumulative orientation error distribution is sufficient for both monotonicity of spatial throughput (Prop. 3) and unimodality of transmission capacity (Prop. 5) when

expressed as functions of antenna beamwidth. A comparison of our analytical results with that of numerical results involving more complex radiation patterns is provided in §VI. We conclude our work and outline future avenues of research in §VII. Finally, for clarity, long proofs are presented in the Appendix.

II. MODEL

We model a wireless network with $\hat{\Phi} = \{(x_i, m_i)\}$, a marked, homogeneous, bipolar Poisson Point Process (PPP) of intensity $\lambda > 0$. $\hat{\Phi}$ models the placement and orientation of transmitter-receiver pairs, where the members of each pair are separated by distance parameter $d > 0$. The ground set $\{x_i\} \subset \mathbb{R}^2$ represents the transmitter (TX) locations, while the *i.i.d.* marks $\{m_i\}$ (formally defined in §II-C) encode the receiver (RX) locations and antenna orientation errors. For notational convenience, we will denote the resulting RX locations with $\{y_i\} \subset \mathbb{R}^2$, where RX i is associated (paired) with TX i . In the following subsections, we detail the rest of our model.

A. Gain Patterns

Each TX and RX is equipped with a 2-dimensional antenna gain pattern $G : [-\pi, \pi) \rightarrow \mathbb{R}^+$. The input angle to $G(\cdot)$ is provided relative to the antenna's boresight, or 'forward' direction. For simplicity, we will assume the gain pattern is symmetric about the boresight angle: $G(-\theta) = G(\theta)$. Further, we will consider parameterized antenna radiation patterns such that the total radiated power (TRP) remains constant over the parameter space; equivalently, $\int_{-\pi}^{\pi} \frac{G(\theta)}{2\pi} d\theta = 1$.

B. Antenna Orientation & Error

Let $\hat{\theta}_{x,y} = \angle(y-x)$ be the angle of the vector from location x to location y relative to the positive x -axis. Thus, for a given TX-RX pair i , $\hat{\theta}_{x_i,y_i}$ is the orientation of the RX about its paired TX. We assume that each communication device may steer its gain pattern $G(\cdot)$ via a simple rotation of the pattern about the device's location. Thus, under the assumption of perfect orientation, the boresight of antennas on TX i and RX i would be aligned directly along $\hat{\theta}_{x_i,y_i}$ and $\hat{\theta}_{y_i,x_i}$ respectively. However, in order to study the effect of antenna misconfiguration on network performance, we introduce additive error ϵ_x into the orientation of a beam originating from location x , measured relative to the perfect orientation angle. For simplicity, we will consider error distributions symmetric about zero degrees. Finally, let θ_{x_i,y_j} and θ_{y_j,x_i} be the angles between TX i and RX j relative to their respective boresight angle. These angles are the gain input angles used to compute the gain between two communication devices, and can be expressed as:

$$\begin{aligned} \theta_{x_i,y_j} &= \hat{\theta}_{x_i,y_j} - (\hat{\theta}_{x_i,y_i} + \epsilon_{x_i}) \\ \theta_{y_j,x_i} &= \hat{\theta}_{y_j,x_i} - (\hat{\theta}_{y_i,x_i} + \epsilon_{y_j}), \end{aligned} \quad (1)$$

and are visualized by Fig. 2. Note: if $i = j$, the gain input angles between TX-RX pair i are simply $\theta_{x_i,y_i} = -\epsilon_{x_i}$ and $\theta_{y_i,x_i} = -\epsilon_{y_i}$.

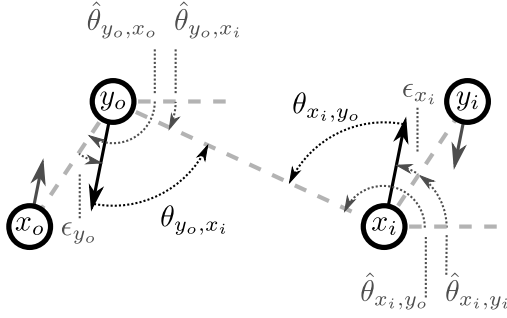


Fig. 2: TX/RX positions are in circles with boresight angles marked by solid arrows. Relevant angles are marked by gray dashed arrows, while gain input angles are black dashed arrows.

C. Marks on the Process

The marks of the process are $\{m_i = (\hat{\theta}_{x_i, y_i}, \epsilon_{x_i}, \epsilon_{y_i})\}$ and consist of the following:

- $\{\hat{\theta}_{x_i, y_i} \sim [-\pi, \pi]\}$, the uniformly distributed orientation of each RX about its paired TX. Note: the marks encode the RX locations $\{y_i\} \subset \mathbb{R}^2$ via $\{\hat{\theta}_{x_i, y_i}\}$ and d ,
- $\{\epsilon_{x_i} \sim f_\epsilon : [-\epsilon_{\max}, \epsilon_{\max}] \rightarrow \mathbb{R}^+\}$, the random orientation error of each TX's beam toward its paired RX, with zero-mean and bounded absolute error $\epsilon_{\max} \leq \pi$, and
- $\{\epsilon_{y_i} \sim f_\epsilon : [-\epsilon_{\max}, \epsilon_{\max}] \rightarrow \mathbb{R}^+\}$, the random orientation error of each RX's beam toward its paired TX, with zero-mean and bounded absolute error $\epsilon_{\max} \leq \pi$.

D. Communication Model

Finally, we model signal propagation using large-scale, distance-based pathloss with Rayleigh fading. The signal power at RX j from TX i is given by:

$$P_{i,j} = P_t H_{i,j} G(\theta_{x_i, y_j}) G(\theta_{y_j, x_i}) d_{i,j}^{-\alpha}, \quad (2)$$

where P_t is a fixed global power assignment across all transmitters, $H_{i,j}$ is the Rayleigh fading coefficient between TX i and RX j with $H_{i,j} \sim \text{Exp}(1)$, $G(\theta_{x_i, y_j})$ and $G(\theta_{y_j, x_i})$ are the gains produced by TX i and RX j respectively in the direction of each other, $\alpha > 2$ is the large-scale pathloss constant, and $d_{i,j}$ is the distance from TX i to RX j (note: $d_{i,i} = d$).

A transmission between TX-RX pair j is considered successful if the signal-to-interference-plus-noise ratio (SINR) falls above a defined SINR threshold $\beta > 0$: $\text{SINR}_j = P_{j,j}/(I_j + \eta)$, where $\eta \geq 0$ is the background noise power and $I_j = \sum_{i \neq j} P_{i,j}$ is the sum interference power at RX j . The probability of success p_s of transmission j is then given by $p_s = \mathbb{P}\{\text{SINR}_j \geq \beta\}$. Unless otherwise noted, common parameters used to generate all figures and numerical results are $\alpha = 3$, $\beta = 4$, $d = 100$ meters, $\eta = 10^{-12}$ Watts, and $P_t = 1$ Watt.

III. A TYPICAL TRANSMISSION

In this section, we discuss the success probability of a typical TX-RX pair o with the receiver located at the origin.

This is possible due to Slivnyak's Theorem (Theorem 8.1 [22]) applied to the PPP $\hat{\Phi}$, which says that the reduced Palm distribution of $\hat{\Phi}$ is equivalent to the original distribution of $\hat{\Phi}$. Here, the reduced Palm distribution of interest first conditions $\hat{\Phi}$ on the locations of x_o and y_o and subsequently removes both points in order to provide analysis on the sum interference generated by $\hat{\Phi}$ and observed at y_o .

A. Induced Gain Distributions

As Wang and Reed [16] note, the antenna gains produced between arbitrary TX/RXs in a PPP are random variables due to their random positions. In this work, we additionally allow the TX/RX orientations to vary independently of their positions via ϵ_{x_i} and ϵ_{y_i} . As a consequence, the random gains produced between the typical TX-RX pair, denoted G_T and G_R , are:

$$\begin{aligned} G_T(\theta_{x_o, y_o}) &= G_T(\epsilon_{x_o}), & \epsilon_{x_o} &\sim f_{|\epsilon|} \\ G_R(\theta_{y_o, x_o}) &= G_R(\epsilon_{y_o}), & \epsilon_{y_o} &\sim f_{|\epsilon|}. \end{aligned} \quad (3)$$

Equations in (3) are due to the simplification of (1) when $i = j = o$. It is sufficient to consider a distribution on the absolute orientation error, $f_{|\epsilon|}$, due to our assumption of a symmetric gain pattern $G(\cdot)$. Additionally, the random gains produced between an arbitrary TX at x_i and the typical RX at y_o , denoted G_{T_i} and G_{R_i} are:

$$\begin{aligned} G_{T_i}(\theta_{x_i, y_o}), & \theta_{x_i, y_o} \sim [-\pi, \pi] \\ G_{R_i}(\theta_{y_o, x_i}), & \theta_{y_o, x_i} \sim [-\pi, \pi], \end{aligned} \quad (4)$$

due to fact that (1) contains the sum of circular r.v.'s, where one of the summands in each sum ($\hat{\theta}_{x_o, y_o}$ or $\hat{\theta}_{x_i, y_i}$) is uniformly distributed over the circle, thus the sum is also uniformly distributed over the circle [23]. In effect, the above four gains have been expressed independently of the geometry of the points in $\hat{\Phi}$. The distributions on the gains will be useful when computing the success probability of a typical transmission.

Remark 1. *In this paper, we restrict our attention to absolute orientation error c.d.f.s, $F_{|\epsilon|}$, that are twice differentiable and concave over bounded support $[0, \epsilon_{\max}]$ with $\epsilon_{\max} \leq \pi$. Concave distributions are equivalently the set of monotonically decreasing distributions $F''_{|\epsilon|}(x) = f'_{|\epsilon|}(x) \leq 0, \forall x \in (0, \epsilon_{\max})$. This is a reasonable class of distributions to model sources of error, especially if increasingly large errors are expected to occur with decreasing likelihood. The assumption of twice differentiability is made to avoid distracting analytical corner cases. From the assumptions of concavity and the support, it follows that $f_{|\epsilon|}(x) > 0, \forall x \in [0, \epsilon_{\max}]$ and $F_{|\epsilon|}(x) > 0, \forall x \in (0, \epsilon_{\max})$. Finally, we will make use of truncated distributions (e.g., exponential truncated to $[0, \pi]$) and parameterize them by their mean (prior to truncation) in the text and figures.*

B. Success Probability

We begin with Prop. 1, which provides a general formulation of the typical transmission success probability under arbitrary gain patterns and error distributions.

Proposition 1 (Success of a Typical Transmission). *In a network modeled by $\hat{\Phi}$ with intensity $\lambda > 0$, TX-RX separation distance d , gain pattern $G(\cdot)$, pathloss constant $\alpha > 2$, background noise $\eta \geq 0$, SINR threshold β , orientation error distribution $f_{|\epsilon|}$, and Rayleigh fading, the success probability p_s of a typical transmission can be expressed as:*

$$p_s = \int_{0^+}^{\infty} \int_{0^+}^{\infty} \exp\left(-\lambda\pi\kappa\left(\frac{\beta}{g_T g_R}\right)^{2/\alpha} \mathbb{E}[G_{T_1}^{2/\alpha}] \mathbb{E}[G_{R_1}^{2/\alpha}] d^2\right) * \exp\left(-\frac{\beta d^\alpha \eta}{P_t g_T g_R}\right) f_{G_T}(g_T) f_{G_R}(g_R) dg_T dg_R, \quad (5)$$

where $\kappa = \Gamma(1 + 2/\alpha)\Gamma(1 - 2/\alpha)$ and both $\mathbb{E}[G_{T_1}^{2/\alpha}]$ and $\mathbb{E}[G_{R_1}^{2/\alpha}]$ are the $2/\alpha$ -moments of the random gains produced between an arbitrary interferer and the typical RX.

As Wang and Reed [16] note, the joint gain distribution $f_{G_{T_1}}(g_{T_1}) f_{G_{R_1}}(g_{R_1})$ can be interpreted as a thinning probability. The expression $\lambda f_{G_{T_1}}(g_{T_1}) f_{G_{R_1}}(g_{R_1})$ represents the intensity of transmitters from $\hat{\Phi}$ that produce a combined gain of $g_{T_1} g_{R_1}$ with the typical receiver at y_o . Further, if we ignore fading and approximate the sum interference (I_o) with the dominant interference,¹ success under each such thinned PPP would require that no interferers exist within a void zone of radius $\left(\beta \frac{g_{T_1} g_{R_1}}{g_T g_R}\right)^{1/\alpha} d$ around the typical receiver. The integral inside the exponent can be interpreted as a product of void probabilities across the independent, thinned PPPs.

With the appropriate assumptions, Prop. 1 can be related back to the success probability under omni-directional antennas [18].

Corollary 1 (Success with Omni-directional Antennas [18]). *Let an omni-directional antenna be described by $G(\theta) = 1, \forall \theta \in [-\pi, \pi]$. If such antennas are employed in a network described by Prop. 1, the success probability p_s of a typical TX-RX pair is: $p_s = e^{-\lambda\pi\kappa\beta^{2/\alpha} d^2} e^{-\frac{\beta d^\alpha \eta}{P_t}}$, where $\kappa = \Gamma(1 + 2/\alpha)\Gamma(1 - 2/\alpha)$.*

Proof: Under omni-directional antennas $G(\theta) = 1$, the four gain distributions are equivalently: $G_T \sim G_R \sim G_{T_1} \sim G_{R_1} \sim f_G(g) = \delta(g-1)$, where $\delta(\cdot)$ is the Dirac delta function. It immediately follows that $\mathbb{E}[G_{T_1}^{2/\alpha}] = \mathbb{E}[G_{R_1}^{2/\alpha}] = 1$. Finally, apply these gain distributions and moments into (5) of Prop. 1. ■

C. Ideal Sectors

Let $G_{\text{ideal}}(\theta)$ be an ideal sector antenna with a gain pattern defined by beamwidth $\omega \in (0, 2\pi)$, main beam gain g_1 , and sidelobe gain g_2 with $0 \leq g_2 < 1 < g_1$:

$$G_{\text{ideal}}(\theta) = \begin{cases} g_1 = \frac{2\pi - (2\pi - \omega)g_2}{\omega} & \text{if } |\theta| \leq \omega/2 \\ g_2 & \text{else} \end{cases}. \quad (6)$$

A visualization of this pattern is provided in Fig. 3. Note: the TRP of (6) is held constant at P_t over the parameter space

¹See Prop. 3.6 and Prop 4.2 from [24]. Under these assumptions, κ can be effectively treated as 1.

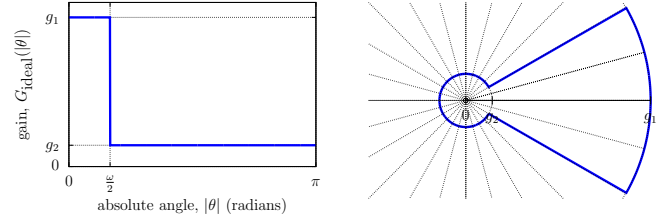


Fig. 3: A symmetric, sector pattern with beamwidth ω , main-beam gain g_1 , and sidelobe gain g_2 .

of ω and g_2 . Lem. 1 provides the four distributions and $2/\alpha$ -moments of the sector pattern gains between the typical RX and both the typical TX and an arbitrary interfering TX.

Lemma 1 (Ideal Sector Gain Distributions). *In a network modeled by $\hat{\Phi}$ with ideal sector antennas described by (6), the gain distributions are given by:*

$$f_{G_T}(g) = f_{G_R}(g) = \bar{u}\delta(g - g_2) + u\delta(g - g_1), \quad (7)$$

$$f_{G_{T_1}}(g) = f_{G_{R_1}}(g) = \bar{p}\delta(g - g_2) + p\delta(g - g_1), \quad (8)$$

where $p = \frac{\omega}{2\pi}$, $\bar{p} = 1 - p$, $u = F_{|\epsilon|}(\omega/2)$ and $\bar{u} = 1 - u$. Further, the $2/\alpha$ -moments of the gain distributions between an arbitrary interferer and the typical receiver are:

$$\mathbb{E}[G_{T_1}^{2/\alpha}] = \mathbb{E}[G_{R_1}^{2/\alpha}] = \bar{p}g_2^{2/\alpha} + pg_1^{2/\alpha}. \quad (9)$$

Proof: Apply the ideal sector pattern (6) to the gain distributions in (3) and (4). Since (6) produces either gains g_1 and g_2 over all possible input angles, the resulting gain distributions are discrete. The moments of the discrete gain r.v.'s are readily computed. ■

We note that p and \bar{p} can be interpreted as the main beam hit rate and miss rate, respectively, between interferers and the typical receiver ultimately due to their uniform orientation with respect to one another. On the other hand, u and \bar{u} are the main beam hit and miss rates, respectively, between the typical TX-RX pair solely determined by their orientation errors.

Corollary 2 (Success with Ideal Sectors). *If sectors described by (6) with non-zero sidelobes ($g_2 > 0$) are employed in a network described by Prop. 1, the success probability p_s of a typical TX-RX pair is:*

$$p_s = u^2 e^{-\lambda\pi\kappa\beta^{2/\alpha} d^2} \left(p + \bar{p} \left(\frac{g_2}{g_1} \right)^{2/\alpha} \right)^2 e^{-\frac{\beta d^\alpha \eta}{P_t g_1^2}} + 2u\bar{u} e^{-\lambda\pi\kappa\beta^{2/\alpha} d^2} \left(p \left(\frac{g_1}{g_2} \right)^{1/\alpha} + \bar{p} \left(\frac{g_2}{g_1} \right)^{1/\alpha} \right)^2 e^{-\frac{\beta d^\alpha \eta}{P_t g_1 g_2}} + \bar{u}^2 e^{-\lambda\pi\kappa\beta^{2/\alpha} d^2} \left(p \left(\frac{g_1}{g_2} \right)^{2/\alpha} + \bar{p} \right)^2 e^{-\frac{\beta d^\alpha \eta}{P_t g_2^2}}. \quad (10)$$

where κ , p , \bar{p} , u , and \bar{u} are as defined in Prop. 1 and Lem. 1.

Proof: Apply the gain distributions and moments from Lem. 1 to (5) of Prop. 1. ■

From Cor. 2, the three summands in (10) correspond to cases involving the typical TX and RX; i) both the typical TX and RX hit each other w.p. u^2 , ii) one hits and the other misses w.p. $2u\bar{u}$, or iii) both miss each other w.p. \bar{u}^2 . In each summand, the last exponential term relates to the transmission

failure rate due to noise under Rayleigh fading, $1 - e^{-\frac{\beta d^\alpha \eta}{P_t g_T g_R}}$, and differs due to the gains between the typical TX-RX pair. Finally, in each summand, the first exponential term contains a quadratic term in p and \bar{p} . This term offers some intuitive interpretations once expanded, where p^2 and $2p\bar{p}$ and \bar{p}^2 represent the cases describing the hit/miss interaction between an arbitrary interferer and the typical RX and can be thought of as thinning probabilities of the interferers in $\hat{\Phi}$. If we ignore fading and approximate sum interference with dominant interference, the ratio of variables g_1 and g_2 represent adjustments to void distances/probabilities for the dominant interferer based on its hit/miss interaction with the typical RX.

Finally, if we assume perfect control over the strength of the sidelobes $g_2 = 0$, we can simplify the success probability further, as given by Cor. 3.

Corollary 3 (Success with Ideal Sectors without Sidelobes). *If sectors described by (6) with zero sidelobes ($g_2 = 0$) are employed in a network described by Prop. 1, the success probability p_s of a typical TX-RX pair is:*

$$p_s = u^2 e^{-\lambda \pi \kappa \beta^{2/\alpha} d^2 p^2} e^{-\frac{\beta d^\alpha \eta}{P_t g_1^2}}. \quad (11)$$

Proof: Apply the gain distributions and moments from Lem. 1 to (5). Note: $g_2 = 0$ and the lower limits of the double integration are 0^+ . ■

The results of Cor. 3 offer a nice interpretation when compared to the omni-directional results of Cor. 1. First, an arbitrary interferer and the typical RX will hit each other w.p. p^2 which acts to thin the original process of interferers. Second, within this thinned process, the typical TX-RX pair will hit each other with rate u^2 .

A comparison of the success probabilities established in Cor. 1, Cor. 2, and Cor. 3 can be seen in Fig. 4. The degree to which the success under ideal sector antennas with sidelobes can be approximated by that of sectors without sidelobes greatly depends on the system parameters ω , $F_{|\epsilon|}$, and g_2 . Without orientation error, the three types of radiation patterns in Fig. 4, omni-directional, sectors without sidelobes, and sectors with sidelobes produce neatly ordered success curves. Furthermore, success without sidelobes is the largest because any energy allocated to sidelobes is essentially wasted between the typical TX-RX pair in the absence of orientation error. Finally, $p_s \rightarrow 1$ as the network intensity λ (and interference) approaches zero.

When orientation error is introduced, the success curves in Fig. 4 are no longer guaranteed to be ordered. In fact, the two sector types produce a crossing, where the presence of sidelobes is beneficial in low density networks, but harmful in high density networks. The presence of sidelobes not only allows interference to be generated and received, but also permits successful communications when antennas are misaligned. In low density networks, interference is minimal, resulting in a net benefit from sidelobes. Regardless of the presence of error, sector antennas tend to increase a typical transmission's success for higher spatial intensities λ over that of omni directional antennas. Additionally, sectors with and without sidelobes produce similar success curves when *i*)

the beamwidth is sufficiently larger than the mean orientation error, or *ii*) the sector sidelobe is sufficiently suppressed. As the network intensity λ approaches zero, success of sectors without sidelobes is upper bounded by the typical TX-RX hit rate $u^2 = F_{|\epsilon|}^2(\omega/2)$ which decreases as the beamwidth narrows.

IV. MAXIMIZING SPATIAL THROUGHPUT

The *spatial throughput* of a network described by Prop. 1 is the maximum spatial intensity of successful transmissions. Spatial throughput (TP) is found by the maximization of $\lambda p_s(\lambda)$ over the spatial intensity of active transmitters λ :

$$\text{TP} = \max_{\lambda > 0} \lambda p_s(\lambda). \quad (12)$$

Spatial throughput can be achieved by an appropriate trade-off of the intensity of active transmitters λ with the transmission success rate $p_s(\lambda)$ (a monotone decreasing function of λ). Prop. 2 provides the optimal spatial intensity of active transmitters λ^* and the resulting success rate $p_s(\lambda^*)$ that achieves TP for networks that employ ideal sector without sidelobes.

Proposition 2 (TP using Sectors without Sidelobes). *If sectors described by (6) with zero sidelobes ($g_2 = 0$) are employed in a network described by Prop. 1, the network's spatial throughput is $\text{TP}_s = \lambda^* p_s(\lambda^*)$, where:*

$$p_s(\lambda^*) = u^2 e^{-1 - \frac{\beta d^\alpha \eta}{P_t g_1^2}}, \quad \lambda^* = \frac{1}{p^2 \pi \kappa d^2 \beta^{2/\alpha}}. \quad (13)$$

Examining Prop. 2, the dependence of $p_s(\lambda^*)$ and λ^* on ω is such that $p_s(\lambda^*) \rightarrow 0$ and $\lambda^* \rightarrow \infty$ as the beamwidth is decreased $\omega \rightarrow 0$. It stands to reason that if $p_s(\lambda)$ decreases slowly enough in ω , the product (spatial throughput) may be driven higher by a narrowing beamwidth. Along these lines, we have found that spatial throughput TP_s can be increased arbitrarily, despite the presence of orientation error, under the class of concave, twice differentiable error distributions $F_{|\epsilon|}$. This notion is formalized by Prop. 3.

Proposition 3 (Concave $F_{|\epsilon|}$ Implies Monotonicity of TP_s in Beamwidth). *Let sectors described by (6) with zero sidelobes ($g_2 = 0$) be employed in a network described by Prop. 1. If the orientation error c.d.f. $F_{|\epsilon|}$ is concave over $[0, \pi]$, then TP_s is monotone increasing as $\omega \rightarrow 0$.*

In the proof of Prop. 3, we use the fact that concavity of $F_{|\epsilon|}$ implies $\frac{f_{|\epsilon|}(x)}{F_{|\epsilon|}(x)} \leq \frac{1}{x}$ before establishing TP_s monotonicity, producing the following nested subsets of error distributions:

$$\begin{aligned} & \{F_{|\epsilon|} : F_{|\epsilon|} \text{ concave, twice diff.}\} \subset \\ & \left\{ F_{|\epsilon|} : \frac{f_{|\epsilon|}(x)}{F_{|\epsilon|}(x)} \leq \frac{1}{x}, \forall x > 0 \right\} \subset \\ & \{F_{|\epsilon|} : \text{TP}_s \text{ monotone}\}. \end{aligned} \quad (14)$$

The ratio, $\frac{f_{|\epsilon|}}{F_{|\epsilon|}} = \frac{d}{dx} \log(F_{|\epsilon|})$, is also known as the logarithmic derivative of $F_{|\epsilon|}$. We point out that truncations of a distribution $F_{|\epsilon|}$ are simply a linear scaling, and thus preserve concavity and leave the logarithmic derivative of $F_{|\epsilon|}$

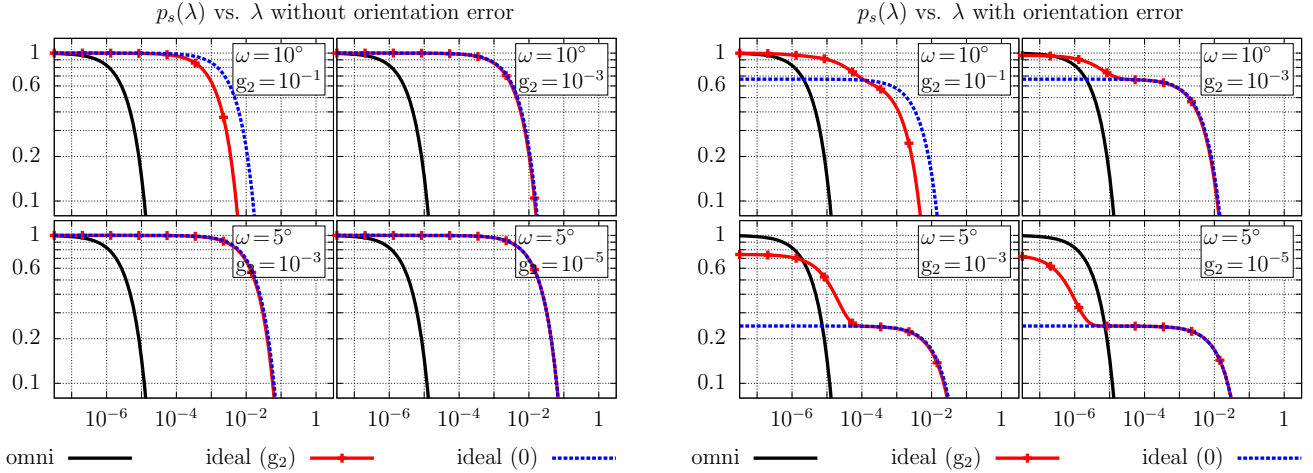


Fig. 4: Sample success curves $p_s(\lambda)$ plotted against intensity of active transmitters λ . Orientation error $|\epsilon|$ is set to zero in the left set of grouped plots; in the right set of grouped plots, orientation error $|\epsilon|$ is modeled using a half-normal distribution with mean $\bar{\epsilon} = 3$ degrees. Curves include the cases of **omni**-directional antennas; **ideal** sector antennas with sidelobes (g_2) with beamwidth ω and sidelobe gain g_2 specified in each subplot; and ideal sector antennas without sidelobes ($g_2 = 0$) with the indicated beamwidth ω specified in each subplot.

unchanged. As a result, we can classify some error distributions with infinite support (e.g., exponential) as satisfying Prop. 3 without having to first truncate them. It is worth noting the possible connection with log-concavity for probability distributions, a well studied subject [25].

A sample of *c.d.f.s* in the class covered by Prop. 3 are the uniform, exponential, and normal *c.d.f.s*, all of which are concave, as stated by Cor. 4.

Corollary 4 (Error Distributions with Monotone TP_s). *If sectors described by (6) with zero sidelobes ($g_2 = 0$) are employed in a network described by Prop. 1 with orientation error modeled by either i) uniform, ii) exponential, or iii) half-normal distributions, then TP_s is monotone decreasing in ω over $[0, 2\pi]$.*

Proof: It is enough to show that $F_{|\epsilon|}(x)$ is concave over $x \in [0, \pi]$ (omitted for brevity). By Prop. 3, it follows that $\text{TP}_s(\omega)$ is monotone decreasing in ω over $(0, 2\pi]$. ■

Remark 2. *While sufficient, concavity of the error distribution $F_{|\epsilon|}$ is not necessary for throughput monotonicity. Consider the following error distribution on $[0, \pi]$ with a ‘dimple’ at (a, b) :*

$$F_{|\epsilon|}(x) = \begin{cases} \frac{b(1-e^{-c_1x})}{1-e^{-c_1a}} & 0 \leq x \leq a \\ b + \frac{(1-b)(1-e^{-c_2(x-a)})}{1-e^{-c_2(\pi-a)}} & a < x \leq \pi \end{cases} \quad (15)$$

Fig. 5 displays (15) with parameter values such that $F_{|\epsilon|}$ is non-concave. However, the example satisfies $\frac{xf_{|\epsilon|}(x)}{F_{|\epsilon|}(x)} \leq 1, \forall x > 0$ and thus yields monotone TP_s .

For completeness, Cor. 5 provides the spatial throughput for networks employing omni-directional antennas, a well studied scenario [18], [24].

Corollary 5 (TP using Omni-directional Antennas). *If omni-directional antennas are employed in a network described by*

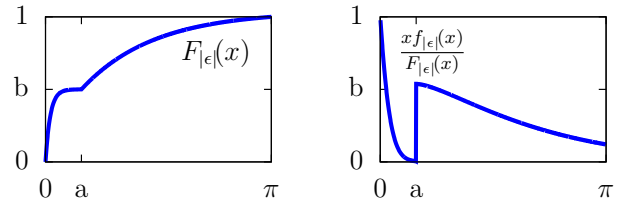


Fig. 5: Sample distribution $F_{|\epsilon|}(x)$ given by (15) with $a = 0.5$, $b = 0.5$, $c_1 = 15$, $c_2 = 1$.

Prop. 1, the network’s spatial throughput is $\text{TP}_0 = \lambda^* p_s(\lambda^*)$, where: $p_s(\lambda^*) = e^{-1 - \frac{\beta d^\alpha \eta}{P_t}}$ and $\lambda^* = \frac{1}{\pi \kappa d^2 \beta^2 / \alpha}$.

Comparing Prop. 2 and Cor. 5 when background noise is negligible ($\eta \approx 0$), the gain in TP by the use of sectors without sidelobes over omni-directional antennas is:

$$\frac{\text{TP}_s}{\text{TP}_0} = \frac{u^2}{p^2} \propto \frac{F_{|\epsilon|}^2(\omega/2)}{\omega^2}, \quad (16)$$

after expanding g_1 , u , and p in terms of ω . As the main beam becomes narrower and stronger, $\omega \rightarrow 0$, the TP gain is affected by decreasing beamwidth in two opposing ways. First, the optimal spatial intensity of active transmitters is increased by factor $p^2 = \frac{4\pi^2}{\omega^2}$ equal to the interferer thinning probability. Second, the success rate at this intensity decreases by factor $u^2 = F_{|\epsilon|}^2(\omega/2)$ equal to the hit rate of the typical TX/RX pair. In the absence of orientation error ($u = 1$), the use of sectorized transmitters with omni-directional receivers produces a TP gain of $1/p \propto 1/\omega$, which mirrors similar throughput gains derived by C.-J. Chang and J.-F. Chang [6].

V. MAXIMIZING TRANSMISSION CAPACITY

Spatial throughput is often achieved by increasing the spatial intensity of active transmitters at the expense of the success

rate of the transmissions. The *transmission capacity* (TC) of a network described by Prop. 1 is the maximum spatial intensity of successful transmissions subject to a maximum outage constraint p_e :

$$\text{TC} = \max_{\lambda > 0, p_s(\lambda) \geq 1 - p_e} \lambda p_s(\lambda). \quad (17)$$

As it has been well established for transmission capacity [24], the monotonicity of p_s in λ allows us to solve this maximization by taking the inverse of $p_s(\lambda)$, which yields the intensity of active transmitters that achieves success rate $1 - p_e$:

$$\text{TC} = \lambda(p_e)(1 - p_e). \quad (18)$$

Prop. 4 extends the analysis of transmission capacity to networks with orientation error and ideal sector antennas without sidelobes.

Proposition 4 (TC using Sectors without Sidelobes). *If sectors described by (6) with zero sidelobes ($g_2 = 0$) are employed in a network described by Prop. 1, the transmission capacity subject to maximum outage p_e is given by $\text{TC}_s = \lambda^*(1 - p_e)$ where:*

$$\lambda^* = \frac{\log\left(\frac{u^2(1-p_{\eta,s})}{1-p_e}\right)}{p^2 \pi \kappa d^2 \beta^{2/\alpha}}, \quad (19)$$

and $p_{\eta,s} = 1 - e^{-\frac{\beta d^\alpha \eta}{P_t g_1^2}}$ is the failure rate due to background noise under Rayleigh fading.

Unlike the monotonicity results obtained for spatial throughput in §IV, the additional outage constraint of transmission capacity combined with antenna orientation error prohibits TC_s from being monotone increasing with the narrowing of antenna beamwidth $\omega \rightarrow 0$. Ignoring background noise ($\eta \approx 0$) for the moment, the argument to the logarithm in (19) is $F_{|\epsilon|}^2(\frac{\omega}{2}) / (1 - p_e)$ when expanded in terms of ω . It follows that when $\omega < 2F_{|\epsilon|}^{-1}(\sqrt{1 - p_e})$, the transmission capacity expression will be negative, $\text{TC}_s < 0$. This can be interpreted in the following manner: there is a minimum threshold for beamwidth, beyond which the typical TX/RX hitting probability u^2 becomes smaller than the required success rate $1 - p_e$. In this beamwidth regime, the transmission capacity outage constraint cannot be satisfied simply due to typical TX/RX misalignment, and transmission capacity can effectively be considered zero.

Along the lines of maximizing TC_s as a function of antenna beamwidth, we have found that transmission capacity TC_s is unimodal in ω under the class of concave, twice differentiable error distributions $F_{|\epsilon|}$. This notion is formalized by Prop. 5.

Proposition 5 (Concavity of $F_{|\epsilon|}$ Implies Unimodality of TC_s). *Let sectors described by (6) with zero sidelobes ($g_2 = 0$) be employed in a network described by Prop. 1 with outage constraint $p_e > 0$. If the orientation error c.d.f. $F_{|\epsilon|}$ is concave over $[0, \pi]$, then there exists a unique maximizer of TC_s within $\omega \in \left(2F_{|\epsilon|}^{-1}(\sqrt{1 - p_e}), 2\epsilon_{\max}\right)$.*

Prop. 5 relies on the fact that TC_s is monotone outside of the stated domain, while being quasi-concave (unimodal) inside, producing a unique maximizer.

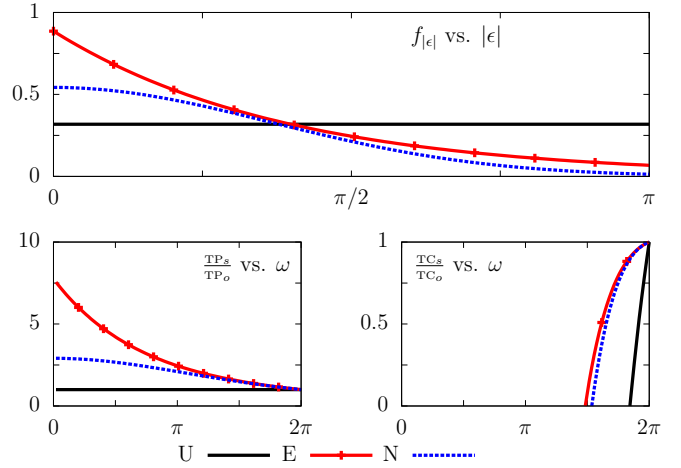


Fig. 6: Sample error *p.d.f.s*, (Uniform, Exponential, and half-Normal) plotted over support $|\epsilon| \in [0, \pi]$ are shown in the top plot. The bottom-left and bottom-right plots display normalized spatial throughput TP_s/TP_o and normalized transmission capacity TC_s/TC_o with outage $p_e = 0.15$ plotted against antenna beamwidth ω , respectively. The Uniform has a mean of $\bar{\epsilon} = 90$ degrees, while the Exponential and half-Normal are assigned a mean of $\bar{\epsilon} = 70$ degrees. Note: the mean must be set large enough to satisfy the first condition of Cor. 6.

Following the results of Prop. 5, the location of the unique maximizer ω^* of TC_s can be expressed based on conditions on $f_{|\epsilon|}$ evaluated at the *r.h.s.* of its support $\omega/2 = \epsilon_{\max}$.

Corollary 6 (Conditions on the Maximizing ω^* for TC_s). *Let sectors described by (6) with zero sidelobes ($g_2 = 0$) be employed in a network described by Prop. 1 with outage constraint $p_e > 0$. If the orientation error c.d.f. $F_{|\epsilon|}$ is concave over $[0, \pi]$, then the unique maximizer ω^* of TC_s has the following properties:*

- If $f_{|\epsilon|}(\epsilon_{\max}) \geq \frac{\log\left(\frac{1-p_e}{\epsilon_{\max}}\right)}{\epsilon_{\max}}$, then $\omega^* = 2\epsilon_{\max}$.
- If $f_{|\epsilon|}(\epsilon_{\max}) < \frac{\log\left(\frac{1-p_e}{\epsilon_{\max}}\right)}{\epsilon_{\max}}$, then $\omega^* \in \left(2F_{|\epsilon|}^{-1}(\sqrt{1 - p_e}), 2\epsilon_{\max}\right)$, and ω^* is the unique solution to the equation:

$$\frac{f_{|\epsilon|}(\omega/2)}{F_{|\epsilon|}(\omega/2)} = \frac{1}{\omega/2} \log\left(\frac{F_{|\epsilon|}^2(\omega/2)}{1 - p_e}\right). \quad (20)$$

Interestingly, Cor. 6 indicates that ω^* depends only on the outage constraint p_e and the error distribution $F_{|\epsilon|}$ and is independent of other system parameters α, β, η, d , and λ .

Remark 3. *Cor. 6 implies that two opposite strategies may be required to separately maximize spatial throughput and transmission capacity. Let $F_{|\epsilon|}$ be concave with $\epsilon_{\max} = \pi$ and let $f_{|\epsilon|}(\epsilon_{\max}) \geq \log\left(\frac{1-p_e}{1-p_e}\right)/\epsilon_{\max}$. By concavity of $F_{|\epsilon|}$, Prop. 3 implies that maximizing spatial throughput is done with $\omega \rightarrow 0$. However, by the additional assumptions on $f_{|\epsilon|}(\epsilon_{\max})$, Cor. 6 implies that maximizing transmission capacity is achieved as $\omega \rightarrow 2\epsilon_{\max} = 2\pi$. Fig. 6 shows error distributions with parameter values such that the (normalized)*

spatial throughput and transmission capacity are maximized by opposite extremes of beamwidth, $\omega \rightarrow 0$ and $\omega \rightarrow 2\pi$.

For completeness, Cor. 7 provides the transmission capacity for networks employing omni-directional antennas, a well studied scenario [24].

Corollary 7 (TC using Omni-directional Antennas). *If omni-directional antennas are employed in a network described by Prop. 1, the transmission capacity subject to maximum outage p_e is $\text{TC}_o = \lambda^*(1 - p_e)$ where $\lambda^* = \frac{\log\left(\frac{1-p_{\eta,o}}{1-p_e}\right)}{\pi\kappa d^2\beta^2/\alpha}$ and $p_{\eta,o} = 1 - e^{-\frac{\beta d^\alpha \eta}{P_t}}$ is the failure rate due to background noise under Rayleigh fading.*

Comparing Prop. 4 and Cor. 7 when background noise is negligible $\eta \approx 0$, we see that sector antennas without sidelobes increase the transmission capacity by a factor of:

$$\frac{\text{TC}_s}{\text{TC}_o} = \frac{1}{p^2} \log\left(\frac{u^2}{1-p_e}\right) \propto \frac{1}{\omega^2} \log\left(\frac{F_{|e|}^2\left(\frac{\omega}{2}\right)}{1-p_e}\right), \quad (21)$$

after expanding g_1 , u , and p in terms of ω . As the main beam becomes narrower and stronger, $\omega \rightarrow 0$, the gain in transmission capacity differs from that of spatial throughput in (16). The success rate is fixed at $1 - p_e$, thus the realized gain is purely a function of an adjustment to the spatial intensity of active transmitters. While this intensity contains a similar factor $1/p^2$ as (16), the numerator is now $\log\left(\frac{F_{|e|}^2(\omega/2)}{1-p_e}\right)$, instead of simply $F_{|e|}^2(\omega/2)$, due to the fixed outage constraint. In the absence of orientation error ($u = 1$) and the employment of sectorized transmitters, the transmission capacity gain is $1/p^2 \propto 1/\omega^2$. When the beamwidth ω is converted into an equivalent number of sectors M covering the circle $\omega = \frac{2\pi}{M}$, we recover similar transmission capacity gains $\Theta(M^2)$ derived by Hunter *et al.* [14].

VI. RESULTS

In this section, we explore the relationship between mean orientation error, throughput maximizing beamwidths, and maximum throughput using sector patterns based on those of *i)* Baccelli and Błaszczyszyn [18] and Akoum *et al.* [17], and *ii)* the spatial channel model used by 3GPP standards [26]. Numerical methods are used to compute the success probability of the typical transmission as well as the derived throughput metrics.

Based on [17], let $G_{\text{trans}}(\theta)$ in (22) be an antenna gain pattern defined by 3dB-beamwidth ω , main beam gain g_1 , and sidelobe gain g_2 with $0 \leq g_2 < g_1$ and transition width γ :

$$G_{\text{trans}}(\theta) = \begin{cases} g_1 = \frac{2\pi - (2\pi - 3/2\gamma - \omega)g_2}{\omega} & \text{if } |\theta| \leq \theta_1 \\ g_1 - \frac{g_1}{\gamma} (|\theta| - \theta_1) & \text{if } \theta_1 < |\theta| \leq \theta_2 \\ \frac{2g_2}{\gamma} (|\theta| - \theta_2) & \text{if } \theta_2 < |\theta| \leq \theta_3 \\ g_2 & \text{if } \theta_3 < |\theta| \leq \pi \end{cases}, \quad (22)$$

with $\theta_1 = \omega/2 - \gamma/2$, $\theta_2 = \omega/2 + \gamma/2$, and $\theta_3 = \omega/2 + \gamma$. In order to yield constant TRP, we place the following restrictions on the pattern's parameterization. The beamwidth

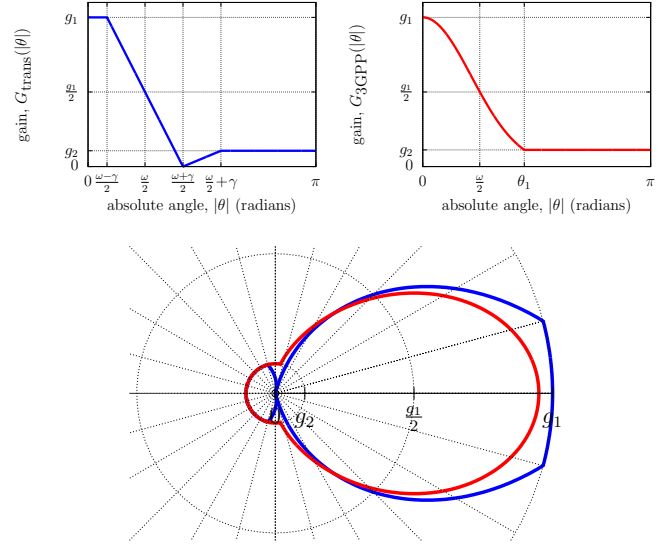


Fig. 7: Sector patterns (22) and (23) (top-left and top-right plots, respectively) with 3-dB beamwidth of ω , transition width γ , mainbeam gain g_1 and sidelobe gain g_2 . Pictured in the bottom plot is a superimposed polar plot of both patterns for common $g_2 = 0.35$ and $\omega = 90$ degrees.

and transition width must jointly satisfy $\omega \in (0, 2\pi - 2\gamma)$ and $\gamma \in (0, \min\{\omega, \pi - \omega/2\})$ so that the full transition from main beam gain g_1 to sidelobe gain g_2 occurs within $|\theta| \in [0, \pi]$. Finally, the sidelobe gain must satisfy $g_2 \in [0, 1/(1 - \frac{3\gamma}{4\pi})]$ in order for the sidelobe to be smaller than the main lobe $g_2 < g_1$. See Fig. 7 for a visualization of this pattern and relevant parameters. As the transition width decreases ($\gamma \rightarrow 0$), we recover the ideal sector pattern from (6) with an identical beamwidth ω .

Based on a 3GPP channel model [26], let $G_{3\text{GPP}}(\theta)$ in (23) be an antenna gain pattern defined by 3dB-beamwidth ω , max gain g_1 , and sidelobe gain g_2 with $0 \leq g_2 < g_1$:

$$G_{3\text{GPP}}(\theta) = \begin{cases} g_1 10^{-\frac{3}{10}\left(\frac{|\theta|}{\omega/2}\right)^2} & \text{if } |\theta| \leq \theta_1 \\ g_2 & \text{if } \theta_1 < |\theta| \leq \pi \end{cases}, \quad (23)$$

with $\theta_1 = \omega/2\sqrt{10/3\log_{10}(g_1/g_2)}$ representing the angle at which the mainbeam falls off to the sidelobe level. Note: g_1 is solved for numerically to yield normalized TRP, and the parameter space of ω and g_2 is necessarily restricted so that θ_1 falls within $[0, \pi]$. See Fig. 7 for a visualization of this pattern and relevant parameters.

In Fig. 8, we compare the network performance of several radiation patterns explored in this paper. The success rate of a typical transmission (top-left of Fig. 8) is provided with inset and outset plots. The inset plot shows that the success curves generally tracked one another closely. The outset plot magnifies differences between the curves that occur at higher success rates ($\geq 95\%$). As the transition width γ is decreased, we observe success rates fall, perhaps due to a ‘broadening’ of the antenna’s main beam that interferes with other transmissions more than it helps cope with orientation

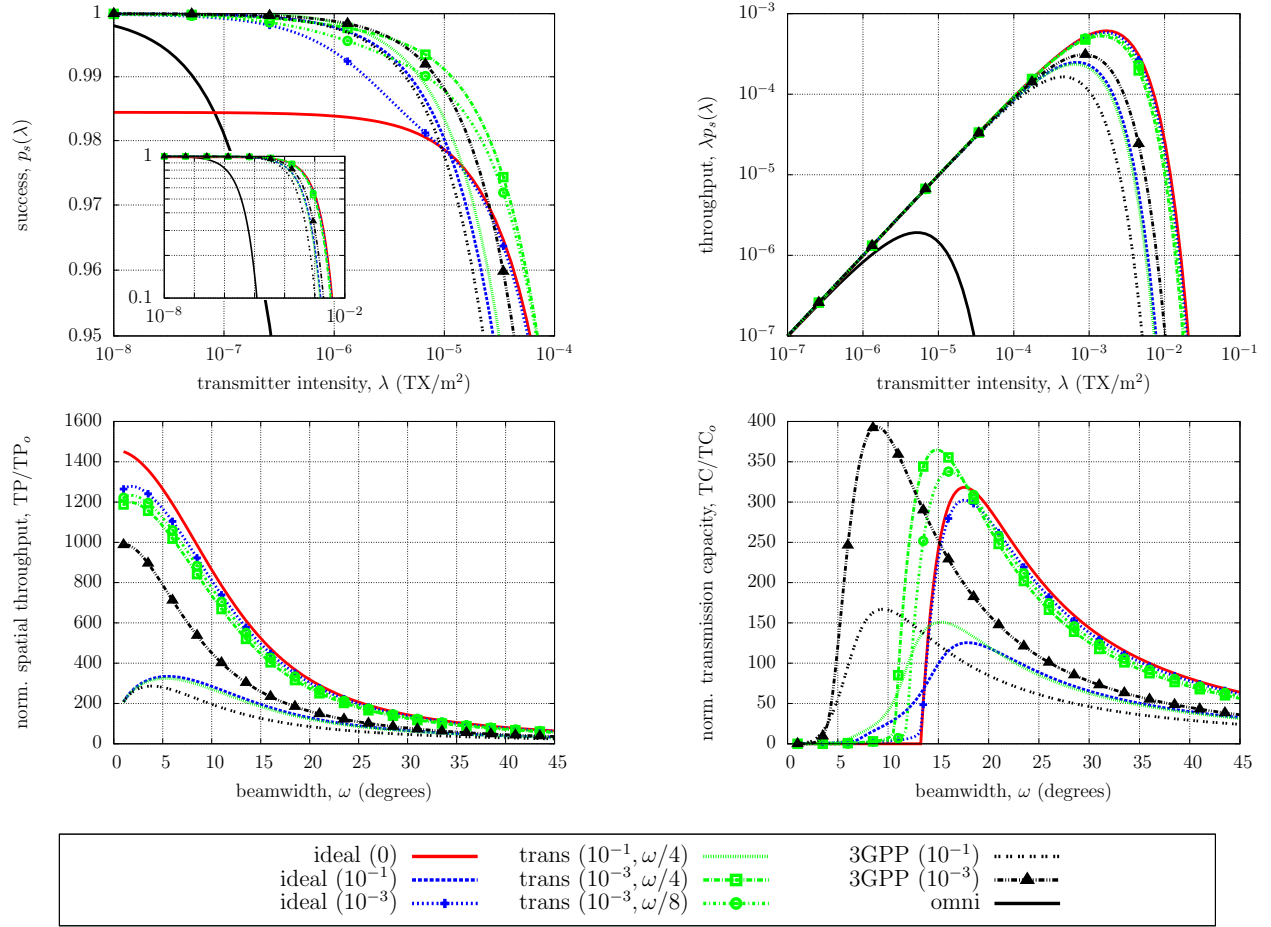


Fig. 8: Plotted are success probability (top-left), throughput as a function of transmitter intensity λ (top-right), throughput maximized over λ (bottom-left), and outage-constrained throughput maximized over λ (bottom-right). The legend includes **omni**-directional antennas; **ideal** sector with sidelobe strength (g_2); sector with sidelobe strength and **transition** width (g_2, γ); and the **3GPP** sector with sidelobe strength (g_2). Default parameters include $p_e = 0.15$, $\omega = 20$ degrees, and $g_2 = 0.1$. Orientation error $|\epsilon|$ is a half-normal distributed *r.v.* with a mean of $\bar{\epsilon} = 3$ degrees.

error. As the sidelobe is decreased for all three sector patterns, the main beam is strengthened and we note increased success under higher TX intensities ($\lambda \geq 10^{-5}$).

The throughput of the network (top-right of Fig. 8) shows the spatial intensity of successful transmissions plotted against TX intensity for a fixed beamwidth of $\omega = 20$ degrees and fixed mean orientation error of $\bar{\epsilon} = 3$ degrees. Higher throughputs are achieved at higher TX intensities using the directional patterns over an omni-directional pattern. At this fixed beamwidth, the sidelobe strength g_2 appears to be the dominant factor (compare with transition width γ) in the behavior of throughput. Throughput curves for all three patterns corresponding to stronger sidelobes ($g_2 = 10^{-1}$) produce lower throughput and maximizing TX intensity than smaller sidelobes ($g_2 = 10^{-3}$).

Spatial throughput (throughput maximized *w.r.t.* λ) plotted against antenna beamwidth ω (bottom-left of Fig. 8), is shown for a fixed mean orientation error. As beamwidth is decreased below 20 degrees, we begin to see a greater differentiation

in TP achieved by each of the evaluated radiation patterns. While the analytical result of TP-monotonicity in Prop. 3 is reflected numerically for ideal sectors without sidelobes ($g_2 = 0$), the introduction of sidelobes and transition widths into the directional radiation pattern does not preserve spatial throughput monotonicity.

Transmission capacity (outage-constrained throughput maximized *w.r.t.* λ) plotted against antenna beamwidth ω (bottom-right of Fig. 8) is also shown for a fixed mean orientation error. For ideal sector patterns, as sidelobes are removed and transition width is narrowed, TC tends to increase and the maximizing ω decreases to match the results obtained by ideal sectors without sidelobes. For the 3GPP pattern, we note that the TC-maximizing beamwidth does not appear to vary with a change in sidelobe strength. Additionally, the TC-unimodality in Prop. 5 is reflected numerically for ideal sectors without sidelobes and appears to hold experimentally for all other shown radiations patterns.

The outage constraint p_e appears to enforce a sharp falloff

in TC as beamwidth narrows (compare with TP). This is explicitly observed in the ideal sector pattern without sidelobes. In this case, missing the main beam, even slightly, provides no throughput benefit. In all patterns with small sidelobes $g_2 = 10^{-3}$, the falloff in TC is very similar with the exception of a tail on the *l.h.s.* The TC-maximizing beamwidth appears more sensitive to the pattern type (ideal, trans, 3GPP) while the maximum TC appears more sensitive to the sidelobe gain $g_2 \in \{10^{-1}, 10^{-3}\}$. Ultimately, the outage constraint prohibits blind throughput maximization *w.r.t.* λ at the expense of success, thus lower throughput is realized with TC versus TP.

In Fig. 9, we explore the maximization of TP and TC (*w.r.t.* beamwidth ω) plotted against mean orientation error (top-left and top-right of Fig. 9, respectively). In general, maximum spatial throughput TP^* and maximum transmission capacity TC^* decrease as the uncertainty in orientation increases and behave rather identically across radiation patterns. For the configurations plotted, the sidelobe strength g_2 is the dominant factor in separating the throughput curves.

The corresponding maximizing beamwidths ω^* for both maximum throughput metrics (bottom-left and bottom-right of Fig. 9) are also plotted against mean orientation error. Intuitively, the TP- and TC-maximizing beamwidths tend to increase with an increased uncertainty in antenna orientation. Also, as expected under ideal sectors without sidelobes, TP-monotonicity results in a maximizing beamwidth of zero regardless of the mean orientation error. The addition of sidelobes and transition widths into the sector pattern produces TP-maximizing beamwidths larger than zero, and the outage-constrained nature of TC^* produces significantly larger optimal beamwidths than TP^* . The sidelobe strength g_2 seems to be the determining factor in grouping TP-maximizing beamwidth curves, while the radiation pattern type (ideal, trans, 3GPP) appears to be the more dominant factor in grouping TC-maximizing beamwidth curves. For the scenarios investigated, the TC-maximizing beamwidth for the ideal sector without sidelobes seems to provide a good approximation for all other ideal sectors with sidelobes and also serves as an upper bound for the remaining patterns (trans and 3GPP).

Remark 4. *Interestingly, we see that both TP- and TC-maximizing beamwidths have a nearly linear relationship with the mean orientation error for all radiation patterns displayed. Assuming truncated exponential orientation error, the optimality constraint (20) can be reparameterized by the ratio $\omega/\bar{\epsilon}$, indicating that ω^* does indeed scale linearly with $\bar{\epsilon}$ under the assumption of ideal sectors without sidelobes.*

VII. CONCLUSIONS & FUTURE WORK

In this paper, we introduced a model for capturing the effects of beam misdirection on coverage and throughput in a directional wireless network using stochastic geometry. In networks employing ideal sector antennas without sidelobes, we found that the moderate assumption of a concave orientation error *c.d.f.* was sufficient to prove monotonicity and quasi-concavity (both with respect to antenna beamwidth) of

spatial throughput (TP) and outage-constrained transmission capacity (TC), respectively. Our numerical results confirm this, but also show that monotonicity of spatial throughput is not preserved for networks employing more complex antenna models. However, unimodality appears to be maintained across the various radiation patterns studied for both throughput metrics, which warrants further investigation.

While varying the sector pattern's sidelobe strength and 'sharpness' of the beamwidth, we found that the ideal sector pattern without sidelobes varied in its ability to approximate more complex patterns. For instance, while the antenna sidelobe strength could greatly influence transmission capacity maximized over antenna beamwidth, the resulting maximizing beamwidths for different sidelobe strengths tended to be well approximated by that of the sector without sidelobes. There exist possible opportunities for upper bounding metrics (*i.e.*, transmission capacity-maximizing beamwidth) for complex radiation patterns by the use of simpler patterns (*i.e.*, ideal sector antenna without sidelobes).

Finally, we noted an apparent linear relationship between mean orientation error and throughput maximizing beamwidths. This held across both throughput metrics and across the sector patterns explored in this paper, suggesting another interesting future direction of inquiry.

APPENDIX

A. Proof of Prop. 1 (Success of a Typical Transmission)

Proof: A transmission is successful when the SINR is greater than or equal to β :

$$p_s = \mathbb{P}\{\text{SINR}_o \geq \beta\} \quad (24)$$

$$\stackrel{(a)}{=} \mathbb{P}\left\{H_{o,o} \geq \frac{\beta d^\alpha}{P_t G_T(\epsilon_{x_o}) G_R(\epsilon_{y_o})} I_o\right\}^* \\ \mathbb{P}\left\{H_{o,o} \geq \frac{\beta d^\alpha \eta}{P_t G_T(\epsilon_{x_o}) G_R(\epsilon_{y_o})}\right\} \quad (25)$$

$$\stackrel{(b)}{=} \int_{0^+}^{\infty} \int_{0^+}^{\infty} \mathbb{E}[e^{-s I_o}] e^{-\frac{\beta d^\alpha \eta}{P_t g_T g_R}} f_{G_T}(g_T) f_{G_R}(g_R) dg_T dg_R \quad (26)$$

- (a) expand $\text{SINR}_i \geq \beta$, isolate $H_{o,o}$, and apply the memoryless property of $H_{o,o}$, and
- (b) marginalize the gains between the typical TX and RX; the first term is the Laplace transform of the interference evaluated at $s = \frac{\beta d^\alpha}{P_t g_T g_R}$; the second term is the *c.c.d.f.* of $H_{o,o}$.

Following Section 5.1.7 of [22], we work with $\mathbb{E}[e^{-s I_o}]$, an expectation over Φ , the fading variables $H_{i,o}$, and the gains between interferers and the typical RX $\{G_{T_i}(\theta_{x_i, y_o})\}$

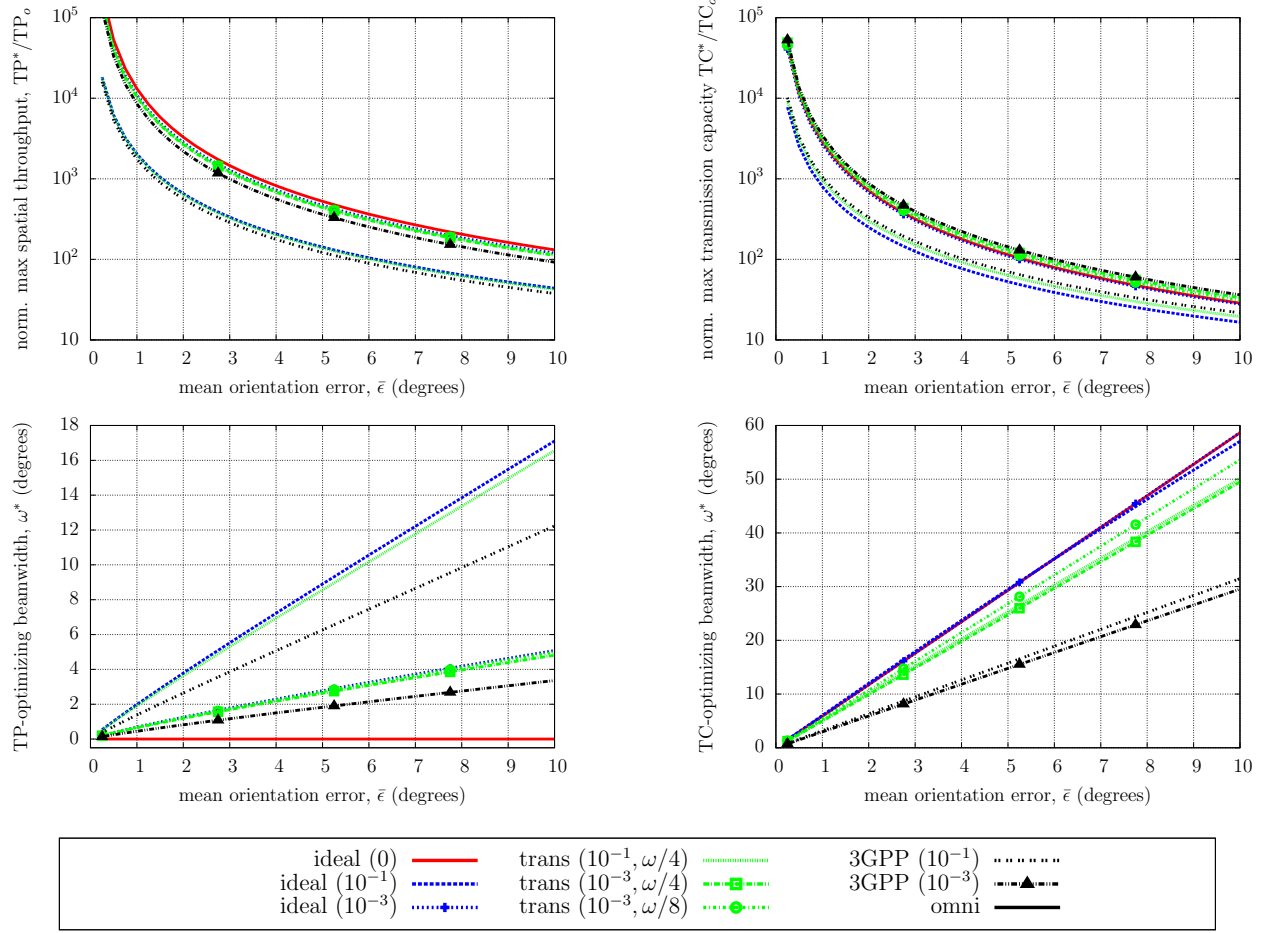


Fig. 9: Plotted are spatial throughput TP maximized over beamwidth (top-left), the resulting TP-maximizing beamwidth (bottom-left), transmission capacity TC maximized over beamwidth (top-right), and the resulting TC-maximizing beamwidth (bottom-right). The legend, default parameters, and orientation error modeling are identical to that of Fig. 8.

and $\{G_{R_i}(\hat{\theta}_{y_o, x_i})\}$:

$$\mathcal{L}_I(s) = \mathbb{E}_{\hat{\Phi}} \left[\prod_{x_i \in \hat{\Phi}} e^{-s P_t G_{T_1}(\hat{\theta}_{x_i, y_o}) G_{R_1}(\hat{\theta}_{y_o, x_i}) H_{i,o} d_{i,o}^{-\alpha}} \right] \quad (27)$$

$$\stackrel{(a)}{=} \mathbb{E}_{\hat{\Phi}} \left[\prod_{x_i \in \hat{\Phi}} \mathbb{E}_{G_{T_1}, G_{R_1}, H} \left[e^{-s P_t G_{T_1} G_{R_1} H d_{i,o}^{-\alpha}} \right] \right] \quad (28)$$

$$\stackrel{(b)}{=} \mathbb{E}_{\hat{\Phi}} \left[\prod_{x_i \in \hat{\Phi}} v(\|x_j\|) \right] \quad (29)$$

$$\stackrel{(c)}{=} e^{-\int_0^\infty 1-v(x)\lambda(x)dx} \quad (30)$$

$$= e^{-\int_0^\infty \mathbb{E}_{G_{T_1}, G_{R_1}, H} \left[1 - e^{-s P_t G_{T_1} G_{R_1} H x^{-\alpha}} \right] \lambda(x) dx} \quad (31)$$

- (a) since x , H , G_{T_1} , and G_{R_1} are all independent from each other, expectations are taken separately and brought into the product, while indexing on the fading and gains is dropped,
- (b) with y_o at the origin, we collapse $\hat{\Phi}$ into a one-dimensional PPP on \mathbb{R}^+ with intensity $\lambda(x) = \lambda 2\pi x, \forall x \in \mathbb{R}^+$ and define $v(x) =$

$$\mathbb{E}_{G_{T_1}, G_{R_1}, H} \left[e^{-s P_t G_{T_1} G_{R_1} H x^{-\alpha}} \right], \text{ and}$$

- (c) a mean of a product of $v(x)$ over the collapsed $\hat{\Phi}$ is a probability generating functional (pgfl) of the process; an explicit solution is given by Campbell's Theorem for PPPs.

Again mirroring the developments in [22], we work with the integral inside the exponential, x , G_{T_1} , G_{R_1} , and H are independent, so their expectations can be evaluated separately:

$$\int_0^\infty \mathbb{E}_{G_{T_1}, G_{R_1}, H} \left[1 - e^{-s P_t G_{T_1} G_{R_1} H x^{-\alpha}} \right] \lambda(x) dx \quad (32)$$

$$\stackrel{(a)}{=} \mathbb{E}_{G_{T_1}, G_{R_1}, H} \left[\int_0^\infty (1 - e^{-s P_t G_{T_1} G_{R_1} H x^{-\alpha}}) \lambda(x) dx \right] \quad (33)$$

$$= \mathbb{E}_{G_{T_1}, G_{R_1}, H} \left[\lambda \pi \int_0^\infty (1 - e^{-s P_t G_{T_1} G_{R_1} H x^{-\alpha}}) 2x dx \right] \quad (34)$$

$$\stackrel{(b)}{=} \mathbb{E}_{G_{T_1}, G_{R_1}} \left[\lambda \pi \Gamma(1 + 2/\alpha) \Gamma(1 - 2/\alpha) (s P_t G_{T_1} G_{R_1})^{2/\alpha} \right] \quad (35)$$

$$\stackrel{(c)}{=} \lambda \pi \Gamma(1 + 2/\alpha) \Gamma(1 - 2/\alpha) (s P_t)^{2/\alpha} \mathbb{E} \left[G_{T_1}^{2/\alpha} \right] \mathbb{E} \left[G_{R_1}^{2/\alpha} \right] \quad (36)$$

- (a) exchange the order of integration over G_{T_1} , G_{R_1} , and H with that of x ,
- (b) as done in Section 5.1.7 of [22] in the case of Rayleigh fading with omni-directional antennas, the substitution of the integration variables, integration by parts, evaluation of the resulting integral, and finally taking the expectation over H produces:

$$\begin{aligned} \mathbb{E}_H \left[\lambda c_d \int_0^\infty (1 - e^{-\hat{s} H x^{-\alpha}}) dx^{d-1} dx \right] \\ = \lambda c_d \Gamma(1 + \delta) \Gamma(1 - \delta) \hat{s}^\delta \end{aligned} \quad (37)$$

where d is the dimension of the space in which the points of Φ reside, $\delta = d/\alpha$ and c_d is a constant depending on d .

In our case, $d = 2$ and it follows that $\delta = 2/\alpha$ and $c_2 = \pi$. By substituting $\hat{s} = s P_t G_{T_1} G_{R_1}$ and taking the expectation of both sides of (37) *w.r.t.* G_{T_1} and G_{R_1} , we complete this step.

- (c) expectations over G_{T_1} and G_{R_1} reduce to taking moments of each *r.v.*, (as noted in [16]).

Now, the Laplace transform can be expressed:

$$\begin{aligned} \mathcal{L}_I(s) &= \mathbb{E} [e^{-s I_o}] \\ &= e^{-\lambda \pi \Gamma(1+2/\alpha) \Gamma(1-2/\alpha) (s P_t)^{2/\alpha} \mathbb{E}[G_{T_1}^{2/\alpha}] \mathbb{E}[G_{R_1}^{2/\alpha}]} \end{aligned} \quad (38)$$

$$(39)$$

With $s = \frac{\beta d^\alpha}{P_t g_T g_R}$, we express success probability of a transmission between the typical pair o :

$$\begin{aligned} p_s &= \int_{0^+}^\infty \int_{0^+}^\infty \mathbb{E}[e^{-s I_o}] e^{-\frac{\beta d^\alpha \eta}{P_t g_T g_R}} f_{G_T}(g_T) f_{G_R}(g_R) dg_T dg_R \\ &= \int_{0^+}^\infty \int_{0^+}^\infty e^{-\lambda \pi \Gamma(1+2/\alpha) \Gamma(1-2/\alpha) (s P_t)^{2/\alpha} \mathbb{E}[G_{T_1}^{2/\alpha}] \mathbb{E}[G_{R_1}^{2/\alpha}]} \\ &\quad e^{-\frac{\beta d^\alpha \eta}{P_t g_T g_R}} f_{G_T}(g_T) f_{G_R}(g_R) dg_T dg_R. \end{aligned} \quad (40)$$

$$(41)$$

B. Proof of Prop. 2 (TP using Sectors without Sidelobes)

Proof: The first and second derivatives of $\lambda p_s(\lambda)$ are:

$$\frac{d}{d\lambda} \lambda p_s(\lambda) = (1 - A\lambda) C e^{-\lambda A - B} \quad (42)$$

$$\frac{d^2}{d\lambda^2} \lambda p_s(\lambda) = (A\lambda - 2) A C e^{-\lambda A - B}, \quad (43)$$

where $A = \pi \kappa d^2 \beta^{2/\alpha} p^2$, $B = \frac{\beta d^\alpha \eta}{P_t g_1^2}$, and $C = u^2$. A single root of the first derivative exists at $\lambda^* = 1/A$, while the second derivative, when evaluated at λ^* , is negative:

$$\left. \frac{d^2}{d\lambda^2} \lambda p_s(\lambda) \right|_{\lambda=\lambda^*} = -A C e^{-1-B} \leq 0, \quad (44)$$

due to $A > 0$, $e^{-1-B} > 0$, and $C = u^2 = F_{|\epsilon|}^2(\frac{\omega}{2}) > 0$ when $\omega > 0$. Thus, due to the first and second derivative tests, we have that λ^* is the global maximizer of $\lambda p_s(\lambda)$. ■

C. Proof of Prop. 3 (Concave $F_{|\epsilon|}$ Implies Monotonicity of TP_s in Beamwidth)

Proof: We rewrite spatial throughput (13) by expanding u , p , g_1 in terms of $x = \omega/2$ and study $TP_s(x)$ over $x \in [0, \pi]$. Specifically, we show that $TP_s(x)$ is monotone decreasing over $(0, \pi]$. To do so, we will need TP_s and its derivative *w.r.t.* x :

$$TP_s(x) = \frac{F_{|\epsilon|}^2(x) e^{-Bx^2}}{Ax^2} \quad (45)$$

$$TP'_s(x) = -\frac{2e^{-Bx^2} F_{|\epsilon|}(x)}{Ax^3} ((1 + Bx^2) F_{|\epsilon|}(x) - x f_{|\epsilon|}(x)), \quad (46)$$

with non-negative constants $A = \frac{1}{\pi} e \kappa d^2 \beta^{2/\alpha}$ and $B = \frac{\beta d^\alpha \eta}{\pi^2 P_t}$.

Since $\frac{2e^{-Bx^2} F_{|\epsilon|}(x)}{Ax^3} > 0$ for all $x \in (0, \pi]$, it suffices to show:

$$0 \leq ((1 + Bx^2) F_{|\epsilon|}(x) - x f_{|\epsilon|}(x)) \quad (47)$$

$$\frac{f_{|\epsilon|}(x)}{F_{|\epsilon|}(x)} \leq \frac{1}{x} + Bx, \quad \forall x \in (0, \pi]. \quad (48)$$

in order to prove spatial throughput is monotone decreasing in x , $TP'_s(x) \leq 0$.

By the assumption of concavity over $[0, \pi]$, $F_{|\epsilon|}$ evaluated at $y \in [0, \pi]$ lies below its first order Taylor series approximation centered at $x \in [0, \pi]$:

$$F_{|\epsilon|}(y) \leq F_{|\epsilon|}(x) + f_{|\epsilon|}(x)(y - x), \quad \forall x, y \in [0, \pi]. \quad (49)$$

After setting $y = 0$, $F_{|\epsilon|}(0) = 0$, rearranging the result, and adding a positive quantity Bx^2 to the *r.h.s.*, we can conclude our proof:

$$\frac{f_{|\epsilon|}(x)}{F_{|\epsilon|}(x)} \leq \frac{1}{x} < \frac{1}{x} + Bx^2, \quad \forall x \in (0, \pi]. \quad \blacksquare \quad (50)$$

D. Proof of Cor. 5 (TP using Omni-directional Antennas)

Proof: The proof of Prop. 2 can be used with $A = \pi \kappa d^2 \beta^{2/\alpha}$, $B = \frac{\beta d^\alpha \eta}{P_t}$, and $C = 1$. Since A , e^{-B} , and C are all positive, $\lambda^* = 1/A$ is the global maximizer of $\lambda p_s(\lambda)$. ■

E. Proof of Prop. 4 (TC with Sectors without Sidelobes)

Proof: Rewrite (11) as $p_s = C e^{-\lambda A - B}$, where $A = \pi \kappa d^2 \beta^{2/\alpha} p^2$, $B = \frac{\beta d^\alpha \eta}{P_t g_1^2}$, and $C = u^2$. Solving for λ yields $\lambda(p_e) = \log\left(\frac{C e^{-B}}{(1-p_e)}\right) / A$. Note that $e^{-B} = 1 - (1 - e^{-B})$, and let $p_\eta = 1 - e^{-B}$, which represents fading outage due to background noise. Multiplying $\lambda(p_e)$ by the success rate $(1 - p_e)$ provides the maximum intensity of successful transmissions, subject to outage p_e . ■

F. Proof of Prop. 5 (Concavity of $F_{|\epsilon|}(\cdot)$ Implies Unimodality of TC_s)

Proof: We rewrite transmission capacity (19) by expanding u , p , g_1 in terms of $x = \omega/2$ and study $TC_s(x)$ over $x \in (0, \pi]$. Specifically, we show that $TC_s(x)$ is *i)* monotone increasing over $(0, x_l]$, *ii)* quasiconcave over $[x_l, x_u]$, and *iii)* monotone decreasing over $(x_u, \pi]$, where $x_l = F_{|\epsilon|}^{-1}(\sqrt{1-p_e})$

and $x_u = \epsilon_{\max}$. Once these three facts are established and combined with the continuity of TC_s over $(0, \pi]$, we can readily conclude that the unique maximizer of TC_s lies between $(x_l, x_u]$ and that TC_s is quasiconcave (unimodal) over this domain. To do so, we will need TC_s and its first two derivatives w.r.t. x :

$$\text{TC}_s(x) = \frac{A}{x^2} (2 \log(F(x)) + B) - AC \quad (51)$$

$$\text{TC}'_s(x) = \frac{2A}{x^2} \left(\frac{f(x)}{F(x)} - \frac{2 \log(F(x)) + B}{x} \right) \quad (52)$$

$$\text{TC}''_s(x) = \frac{2A}{x^3} \left(3 \frac{2 \log(F(x)) + B}{x} - \frac{4f(x)}{F(x)} - \frac{xf(x)^2}{F(x)^2} + \frac{xf'(x)}{F(x)} \right), \quad (53)$$

with positive constants $A = \frac{\pi(1-p_e)}{\kappa d^2 \beta^{2/\alpha}}$, $B = \log\left(\frac{1}{1-p_e}\right)$, and $C = \frac{\beta d^\alpha \eta}{P_t \pi^2}$. Note: TC_s is smooth at x_l and $\text{TC}'_s(x_l) > 0$, but may not be differentiable (i.e., have a sharp turn) at x_u .

For *i*), note that $2 \log(F(x)) + B$ is monotone increasing in x due to the monotonicity of F and \log . It follows that when $x \leq x_l$:

$$2 \log(F(x)) + B \leq 2 \log(F(x_l)) + B \quad (54)$$

$$\leq 2 \log\left(F\left(F_{|\epsilon|}^{-1}\left(\sqrt{1-p_e}\right)\right)\right) + B \quad (55)$$

$$= \log(1-p_e) + \log(1/(1-p_e)) = 0. \quad (56)$$

Substituting this bound into (52), we obtain the desired monotonicity of TC_s :

$$\text{TC}'_s(x) \geq \frac{2A}{x^2} \frac{f(x)}{F(x)} > 0, \quad \forall x \in (0, x_l). \quad (57)$$

For *ii*), we use a sufficient condition for quasiconcavity from Boyd and Vandenberghe [27]:

$$\text{TC}'_s(x) = 0 \Rightarrow \text{TC}''_s(x) < 0, \quad \forall x \in (x_l, x_u). \quad (58)$$

In words, if all stationary points are associated with local maxima, then only a single stationary point exists, which necessarily provides the global maximum. Let $x^* \in (x_l, x_u)$ be a stationary point of TC_s . From (52), $\text{TC}_s(x^*) = 0$ implies:

$$\frac{2 \log(F(x^*)) + B}{x^*} = \frac{f(x^*)}{F(x^*)}. \quad (59)$$

Simplify (53) at this stationary point by substitution of the above equality:

$$\text{TC}''_s(x^*) = \frac{2A}{(x^*)^3} \left(-\frac{f(x^*)}{F(x^*)} - \frac{x^* f(x^*)^2}{F(x^*)^2} + \frac{x^* f'(x^*)}{F(x^*)} \right). \quad (60)$$

$$\left(-\frac{f(x^*)}{F(x^*)} - \frac{x^* f(x^*)^2}{F(x^*)^2} + \frac{x^* f'(x^*)}{F(x^*)} \right). \quad (61)$$

Over (x_l, x_u) , we have $F(x) > 0$, $f(x) > 0$, and $f'(x) \leq 0$, thus $\text{TC}''_s(x^*) < 0$ and TC_s is unimodal over (x_l, x_u) and thus $[x_l, x_u]$ by continuity of TC_s .

For *iii*), note that $F(x) = 1$ and $f(x) = 0$ for all $x > x_u$. Thus, (52) can be simplified:

$$\text{TC}'_s(x) = \frac{-2AB}{x^3} < 0, \quad \forall x \in (x_u, \pi]. \quad (62)$$

Finally, since TC_s is increasing on $(0, x_l]$ and decreasing on $(x_u, \pi]$, the maximization of $\text{TC}_s(x)$ can be reduced to searching over the remaining unimodal portion of TC_s : $(x_l, x_u]$. ■

G. Proof of Cor. 6 (Conditions on the Maximizing ω^* for TC_s)

Proof: First, by Prop. 5 and its proof in Appendix F, we know that $\text{TC}_s(x)$ with $x = \omega/2$ is unimodal and contains a unique maximizer within: $x^* \in \left(F_{|\epsilon|}^{-1}\left(\sqrt{1-p_e}\right), \epsilon_{\max}\right]$.

$\text{TC}_s(x)$ may have a sharp turn at $x = \epsilon_{\max}$, so we take the left derivative of TC_s using (52). Since $F(\epsilon_{\max}) = 1$, we have:

$$\text{TC}'_s(\epsilon_{\max}^-) = \lim_{x \rightarrow \epsilon_{\max}^-} \text{TC}'_s(x) \quad (63)$$

$$= \frac{2A}{\epsilon_{\max}^2} \left(f(\epsilon_{\max}) - \frac{B}{\epsilon_{\max}} \right), \quad (64)$$

with positive constants $A = \frac{\pi(1-p_e)}{\kappa d^2 \beta^{2/\alpha}}$, $B = \log\left(\frac{1}{1-p_e}\right)$.

First, when $f(\epsilon_{\max}) < \frac{B}{\epsilon_{\max}}$, we have $\text{TC}'_s(\epsilon_{\max}^-) < 0$ and the maximizing x^* must lie strictly less than ϵ_{\max} . Second, when $f(\epsilon_{\max}) > \frac{B}{\epsilon_{\max}}$, we have $\text{TC}'_s(\epsilon_{\max}^-) > 0$ and the maximizing x^* must be exactly ϵ_{\max} due to the unimodality of TC_s over the rest of $\left(F_{|\epsilon|}^{-1}\left(\sqrt{1-p_e}\right), \epsilon_{\max}\right]$. Lastly, when $f(\epsilon_{\max}) = \frac{B}{\epsilon_{\max}}$, we have $\text{TC}'_s(\epsilon_{\max}^-) = 0$. We then take the left second derivative of TC_s at ϵ_{\max} using (53), and since ϵ_{\max} is a stationary point of TC_s , we can apply (59):

$$\text{TC}''_s(\epsilon_{\max}^-) = \lim_{x \rightarrow \epsilon_{\max}^-} \text{TC}''_s(x) \quad (65)$$

$$= \frac{2A}{\epsilon_{\max}^3} \left(3 \frac{2 \log(F(\epsilon_{\max})) + B}{\epsilon_{\max}} - \frac{4f(\epsilon_{\max})}{F(\epsilon_{\max})} \right. \quad (66)$$

$$\left. - \frac{\epsilon_{\max} f(\epsilon_{\max})^2}{F(\epsilon_{\max})^2} + \frac{\epsilon_{\max} f'(\epsilon_{\max}^-)}{F(\epsilon_{\max})} \right) \quad (67)$$

$$= \frac{2A}{\epsilon_{\max}^3} \left(-\frac{f(\epsilon_{\max})}{F(\epsilon_{\max})} - \frac{\epsilon_{\max} f(\epsilon_{\max})^2}{F(\epsilon_{\max})^2} + \frac{\epsilon_{\max} f'(\epsilon_{\max}^-)}{F(\epsilon_{\max})} \right) \quad (68)$$

$$= \frac{2A}{\epsilon_{\max}^3} \left(-f(\epsilon_{\max}) - \epsilon_{\max} f(\epsilon_{\max})^2 + \epsilon_{\max} f'(\epsilon_{\max}^-) \right) \quad (69)$$

where $F(\epsilon_{\max}) = 1$. Since $\epsilon_{\max} > 0$, $f(\epsilon_{\max}) > 0$, and $f'(\epsilon_{\max}^-) \leq 0$, we conclude that $\text{TC}''_s(\epsilon_{\max}^-) < 0$ and TC_s is concave down at ϵ_{\max}^- . Thus, the maximizing x^* must be exactly ϵ_{\max} due to the unimodality of TC_s over the rest of $\left(F_{|\epsilon|}^{-1}\left(\sqrt{1-p_e}\right), \epsilon_{\max}\right]$. ■

H. Proof of Cor. 7 (TC with Omni-directional Antennas)

Proof: The proof of Prop. 4 can be used with $A = \pi \kappa d^2 \beta^{2/\alpha}$, $B = \frac{\beta d^\alpha \eta}{P_t}$, and $C = 1$. ■

REFERENCES

- [1] R. Ramanathan, J. Redi, C. Santivanez, D. Wiggins, and S. Polit, "Ad hoc networking with directional antennas: A complete system solution," *IEEE J. Sel. Areas Commun.*, vol. 23, no. 3, pp. 496–506, Mar. 2005.
- [2] S. D. Milner, J. Llorca, and C. C. Davis, "Autonomous reconfiguration and control in directional mobile ad hoc networks," *IEEE Circuits Syst. Mag.*, vol. 9, no. 2, pp. 10–26, Jun. 2009.
- [3] J. Yu, Y.-D. Yao, A. F. Molisch, and J. Zhang, "Performance evaluation of CDMA reverse links with imperfect beamforming in a multicell environment using a simplified beamforming model," *IEEE Trans. Veh. Technol.*, vol. 55, no. 3, pp. 1019–1031, May 2006.

- [4] B. Epple, "Using a gps-aided inertial system for coarse-pointing of free-space optical communication terminals," in *Proceedings of the SPIE*, vol. 6304, no. 630418, Sep. 2006.
- [5] B. L. Wilkerson, D. Giggenbach, and B. Epple, "Concepts for fast acquisition in optical communications systems," in *Proceedings of the SPIE*, vol. 6304, no. 63040A, Sep. 2006.
- [6] C.-J. Chang and J.-F. Chang, "Optimal design parameters in a multihop packet radio network using random access techniques," *Elsevier Computer Networks and ISDN Systems*, vol. 11, no. 5, pp. 337–351, May 1986.
- [7] C. Lau and C. Leung, "Throughput of slotted ALOHA channel with multiple antennas and receivers," *IET Electronics Letters*, vol. 28, no. 25, pp. 1540–1542, Dec. 1988.
- [8] A. Spyropoulos and C. S. Raghavendra, "Asymptotic capacity bounds for ad-hoc networks revisited: The directional and smart antenna cases," in *Proceedings of IEEE Globecom*, San Francisco, CA, USA, Dec. 2003, pp. 1216–1220.
- [9] S. Yi, Y. Pei, S. Kalyanaraman, and B. Azimi-Sadjadi, "How is the capacity of ad hoc networks improved with directional antennas?" *Springer Wireless Networks*, vol. 13, no. 5, pp. 635–648, Oct. 2007.
- [10] J. Wang, L. Kong, and M.-Y. Wu, "Capacity of wireless ad hoc network using practical directional antennas," in *Proceedings of the IEEE Wireless Communications and Networking Conference (WCNC)*, Sydney, Australia, Apr. 2010.
- [11] P. Li, C. Zhang, and Y. Fang, "The capacity of wireless ad hoc networks using directional antennas," *IEEE Trans. Mobile Comput.*, vol. 10, no. 10, pp. 1374–1387, Oct. 2011.
- [12] Y. Chen, J. Liu, X. Jiang, and O. Takahashi, "Throughput analysis in mobile ad hoc networks with directional antennas," *Elsevier Ad Hoc Networks*, vol. 11, no. 3, pp. 1122–1135, May 2013.
- [13] P. Gupta and P. R. Kumar, "The capacity of wireless networks," *IEEE Trans. Inf. Theory*, vol. 46, no. 2, Mar. 2000.
- [14] A. M. Hunter, J. G. Andrews, and S. Weber, "Transmission capacity of ad hoc networks with spatial diversity," *IEEE Trans. Wireless Commun.*, vol. 7, no. 12, pp. 5058–5071, Dec. 2008.
- [15] S. Singh, R. Mudumbai, and U. Madhow, "Interference analysis for highly directional 60-GHz mesh networks: The case for rethinking medium access control," *IEEE/ACM Trans. Netw.*, vol. 19, no. 5, pp. 1513–1527, Oct. 2011.
- [16] H. Wang and M. C. Reed, "Tractable model for heterogeneous cellular networks with directional antennas," in *Australian Communications Theory Workshop (AusCTW)*, Feb. 2012, pp. 61–65.
- [17] S. Akoum, O. E. Ayach, and R. W. Heath Jr., "Coverage and capacity in mmwave cellular systems," in *Proceedings of the IEEE Asilomar Conference on Signals, Systems, and Computers (Asilomar)*, Nov. 2012, pp. 688–692.
- [18] F. Baccelli and B. Błaszczyszyn, *Stochastic Geometry and Wireless Networks*, ser. Foundations and Trends in Networking. NOW Publishers, Jan. 2010.
- [19] J. Shen and L. W. Pearson, "The phase error and beam-pointing error in coupled oscillator beam-steering arrays," *IEEE Trans. Antennas Propag.*, vol. 53, no. 1, pp. 386–393, Jan. 2005.
- [20] H. Li, Y.-D. Yao, and J. Yu, "Outage probabilities of wireless systems with imperfect beamforming," *IEEE Trans. Veh. Technol.*, vol. 55, no. 5, pp. 1503–1515, Sep. 2006.
- [21] V. Vakilian, J.-F. Frigon, and S. Roy, "Effects of angle-of-arrival estimation errors, angular spread and antenna beamwidth on the performance of reconfigurable SISO systems," in *Proceedings of the IEEE Pacific Rim Conference on Communications, Computers and Signal Processing (PacRim)*, Victoria, BC, Canada, Aug. 2011, pp. 515–519.
- [22] M. Haenggi, *Stochastic Geometry for Wireless Networks*. Cambridge University Press, 2013.
- [23] K. M.ardia and P. E. Jupp, *Directional Statistics*. New York, NY, USA: John Wiley & Sons, LTD, 2000.
- [24] S. Weber and J. G. Andrews, *Transmission Capacity of Wireless Networks*, ser. Foundations and Trends in Networking. NOW Publishers, Jan. 2012, vol. 5, no. 2-3.
- [25] M. Bagnoli and T. Bergstrom, "Log-concave probability and its applications," *Springer-Verlag Economic Theory*, vol. 26, no. 2, pp. 445–469, Aug. 2005.
- [26] "UMTS; spatial channel model for MIMO simulations," ETSI 3rd Generation Partnership Project (3GPP), Tech. Rep. 25.996 version 11.0.0 Release 11, Sep. 2012, online: <http://www.3gpp.org/DynaReport/25996.htm>.
- [27] S. Boyd and L. Vandenberghe, *Convex Optimization*. Cambridge University Press, 2004.



communications systems.

Jeffrey Wildman received his dual M.S./B.S. degree in electrical engineering from Drexel University in 2009. He has interned and visited with the Wideband Tactical Networking Group at MIT Lincoln Laboratory (2007, 2009), with the Network Operating Systems Technology Group at Cisco Systems, Inc. (2012), and most recently with the Center for Wireless Communications at the University of Oulu, Finland (2013). Jeffrey is currently pursuing a Ph.D. in electrical engineering at Drexel University with interests in the modeling and analysis of wireless



Pedro Henrique Juliano Nardelli received the B.S. and M.Sc. degrees in electrical engineering from the State University of Campinas, Brazil, in 2006 and 2008, respectively. In 2013 he received his doctoral degree from University of Oulu, Finland, and State University of Campinas following a dual-degree agreement. Nowadays he holds a postdoctoral position at University of Oulu, and his studies are mainly focused on the efficiency of wireless networks and spatio-temporal dynamics of complex systems.



Matti Latva-aho was born in Kuivaniemi, Finland in 1968. He received the M.Sc., Lic.Tech. and Dr. Tech (Hons.) degrees in Electrical Engineering from the University of Oulu, Finland in 1992, 1996 and 1998, respectively. From 1992 to 1993, he was a Research Engineer at Nokia Mobile Phones, Oulu, Finland. During the years 1994-1998 he was a Research Scientist at Telecommunication Laboratory and Centre for Wireless Communications at the University of Oulu. Currently he is the Department Chair Professor of Digital Transmission Techniques and Head of Department at the University of Oulu, Department for Communications Engineering. Prof. Latva-aho was Director of Centre for Wireless Communications at the University of Oulu during the years 1998-2006. His research interests are related to mobile broadband wireless communication systems. Prof. Latva-aho has published over 200 conference or journal papers in the field of wireless communications. He has been TPC Chairman for PIMRC06, TPC Co-Chairman for ChinaCom07 and General Chairman for WPMC08. He acted as the Chairman and vice-chairman of IEEE Communications Finland Chapter in 2000-2003.



Steven Weber (SM 1997, M 2003, S 2011) received his B.S. degree in 1996 from Marquette University in Milwaukee, WI, and his M.S. and Ph.D. degrees from The University of Texas at Austin in 1999 and 2003 respectively. He joined the Department of Electrical and Computer Engineering at Drexel University in 2003 where he is currently an associate professor. His research interests are centered around mathematical modeling of computer and communication networks, specifically streaming multimedia and ad hoc networks.